Bioactive Materials 21 (2023) 299–312

Contents lists available at ScienceDirect

Bioactive Materials

journal homepage: www.keaipublishing.com/en/journals/bioactive-materials

A tumor cell membrane-coated self-amplified nanosystem as a nanovaccine to boost the therapeutic effect of anti-PD-L1 antibody

Zhilin Li [a], Hao Cai [a], Zhiqian Li [a], Long Ren [a], Xuelei Ma [a], Hongyan Zhu [a], Qiyong Gong [a,c], Hu Zhang [b], Zhongwei Gu [a], Kui Luo [a,*]

[a] Laboratory of Stem Cell Biology, Department of Radiology, Huaxi MR Research Centner (HMRRC), Department of Biotherapy, Cancer Center, National Clinical Research Center for Geriatrics, Frontiers Science Center for Disease-related Molecular Network, State Key Laboratory of Biotherapy, West China Hospital, Sichuan University, Chengdu, 610041, China

[b] Amgen Bioprocessing Centre, Keck Graduate Institute, Claremont, CA, 91711, USA

[c] Functional and Molecular Imaging Key Laboratory of Sichuan Province, And Research Unit of Psychoradiology, Chinese Academy of Medical Sciences, Chengdu, 610041, China

ARTICLE INFO

Keywords:
Cell membrane
Biomimetic nanosystem
Immunogenic cell death
Immunotherapy
anti-PD-L1 antibody

ABSTRACT

To improve the response rate of immune checkpoint inhibitors such as anti-PD-L1 antibody in immunosuppressive cancers like triple-negative breast cancer (TNBC), induction of immunogenic cell death (ICD) at tumor sites can increase the antigenicity and adjuvanticity to activate the immune microenvironment so that tumors become sensitive to the intervention of immune checkpoint inhibitors. Herein, a self-amplified biomimetic nanosystem, mEHGZ, was constructed by encapsulation of epirubicin (EPI), glucose oxidase (Gox) and hemin in ZIF-8 nanoparticles and coating of the nanoparticles with calreticulin (CRT) over-expressed tumor cell membrane. EPI acts as an ICD inducer, Gox and hemin medicate the cascade generation of reactive oxygen species (ROS) to strengthen the ICD effect, and CRT-rich membrane as "eat me" signal promote presentation of the released antigens by dendritic cells (DCs) to invoke the tumor-immunity cycle. The biomimetic delivery system displays an amplified ICD effect via Gox oxidation, hydroxyl radical generation and glutathione (GSH) depletion. The induced potent ICD effect promotes DCs maturation and cytotoxic T lymphocytes (CTLs) infiltration, reversing an immunosuppressive tumor microenvironment to an immunoresponsive one. Treatment with the nanosystem in combination with anti-PD-L1 antibody results in distinctive inhibition of tumor growth and lung metastasis, supporting that a potent ICD effect can significantly boost the therapeutic efficacy of the anti-PD-L1 antibody. This self-amplified biomimetic nanoplatform offers a promising means of raising the response rate of immune checkpoint inhibitors.

1. Introduction

Immunotherapy by employing immune checkpoint inhibitors (ICIs), such as anti-PD-1/L1 antibodies, has revolutionized the paradigm of cancer treatment in the last decade [1,2]. However, the response rate of ICIs is very poor, and about 10–30% has been reported in the cancer with an immunosuppressive microenvironment such as triple-negative breast cancer (TNBC) [3–5]. It has been revealed that immunogenic cell death (ICD) can activate the immune microenvironment to potentiate the ICI treatment effect [6]. Tumor cells treated with chemotherapeutic agents anthracyclines such as EPI undergo ICD to release tumor associated antigens and danger associated molecular patterns (DAMPs) including calreticulin (CRT), high mobility group box 1 (HMGB1) and adenosine-5′-triphosphate (ATP) [7,8], reversing an immunosuppressive tumor microenvironment to an immunoresponsive one [9,10]. Encouraging therapeutic outcomes have been reported after treatment with a combination of ICIs with ICD [11,12]. However, ICD induced from one single chemotherapeutic agent is not adequate enough to produce persistent immune responses [13,14].

To address this issue, synergy with multiple intervention methods to amplify the ICD effect has been pursued to boost the therapeutic effect of ICIs [15,16]. The ER stress is often harnessed for strengthening the ICD

Peer review under responsibility of KeAi Communications Co., Ltd.
* Corresponding author.
E-mail addresses: hyzhu_hmrrc@126.com (H. Zhu), luokui@scu.edu.cn (K. Luo).

https://doi.org/10.1016/j.bioactmat.2022.08.028
Received 2 May 2022; Received in revised form 14 July 2022; Accepted 22 August 2022

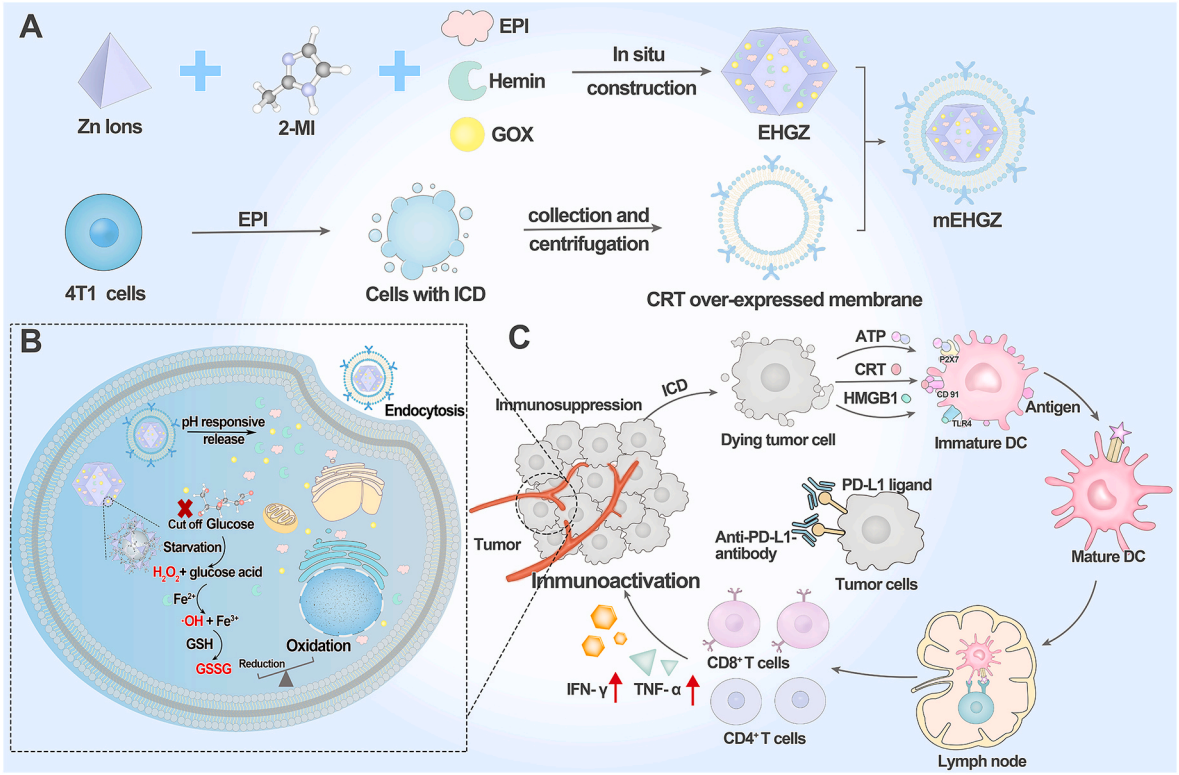

Scheme 1. Construction of a self-amplified biomimetic nanosystem to induce ICD and activate an immune microenvironment for boosting the therapeutic effect of anti-PD-L1 antibody. A) Schematic illustration of the process to prepare mEHGZ nanoparticles by encapsulating EPI, Gox and hemin in ZIF-8 nanoparticles and coating the nanoparticles with the CRT over-expressed tumor cell membrane. B) After endocytosis of mEHGZ nanoparticles into cells, the released EPI from mEHGZ in response to a low pH kills tumor cells in an immunogenic way. Gox and hemin mediate a cascade reaction for generation of hydroxyl free radical (·OH) and depletion of intracellular GSH to exert strong stress on the ER, strengthening the ICD effect. C) The released antigens and DAMPs after ICD promote DCs maturation, $CD8^+$ T cells infiltration and cytokines secretion to create an immunosupportive microenvironment to boost the therapeutic effect of anti-PD-L1 antibody.

effect for potent immunogenic responses. Ca^{2+} depletion, hypoxia, and ROS generation have been proposed to effectively escalate the ER stress, thus inducing ICD [17]. Fenton and Fenton-like reactions are often employed for chemodynamic therapy because intracellular ROS could be generated from these reactions under a specific tumor microenvironment [18]. A glucose oxidase (Gox)-based nanozyme system is safe and efficient to induce Fenton reactions in a quite specific and well-controlled way [19], and this nanozyme can oxidize glucose to gluconic acid and hydrogen peroxide (H_2O_2) in tumor cells. Excess glucose consumption may lead to reduced energy supply to tumor cells, which has been utilized for starvation therapy of cancers. Meanwhile, the product H_2O_2 from glucose oxidation can react with Fe^{2+} via the Fenton reaction to generate hydroxyl radicals (·OH) and oxidize intracellular glutathione (GSH). A reduced level of GSH is often accompanied with a weakening capacity of scavenging of cytotoxic ·OH, thus aggravating the ROS generation and intensifying the ICD effect.

Functionalized nanosized delivery systems have been developed for delivery of therapeutic agents into tumor sites [20,21], and a biomimetic drug delivery system has attracted tremendous attention in recent years [22,23]. Cell membranes from red blood cells [24], platelets [25], natural killer cells [26] and cancer cells [27] have been used for engineering these biomimetic nanoplatforms. Among these cell membranes, the tumor cell membrane can retain the antigens on the cell membrane to evoke immune responses and maintain homotypic adhesion for targeted delivery [28,29]. Besides, CRT on the cell membrane is one of important DAMPs in immunogenic signal transmission, and the presence of CRT promotes engulfment of tumor-associated antigens by antigen-presenting cells (APCs) to activate immune responses. After *in vitro* treatment with tumor cells to stimulate ICD, CRT can be over-expressed on the cell membrane. The use of the cell membrane with over-expressed CRT could strengthen the immunogenicity [30].

Herein, we constructed a biomimetic nanoparticle to trigger a cascade reaction for ROS generation to amplify the ICD effect and boost the sensitivity of tumor cells to the treatment with anti-PD-L1 antibody. In this system, zeolitic imidazolate framework (ZIF-8) nanoparticles were employed as a drug carrier due to their large surface area, porous interconnectivity and intrinsic pH-induced biodegradability. An ICD inducer EPI, Gox and hemin were encapsulated into ZIF-8 nanoparticles to prepare a drug-loaded nanosystem, EHGZ. This EHGZ system was coated with CRT over-expressed tumor cell membrane to obtain a biomimetic nanoparticle, mEHGZ (Scheme 1A). The tumor cell membrane coating layer on mEHGZ could facilitate their cellular uptake by tumor cells and act as an immune adjuvant. After cellular uptake of the mEHGZ nanoparticles, a Fenton reaction could be triggered by released Gox and hemin from mEHGZ nanoparticles to promote ROS generation and elevate the ER stress, which could amplify the ICD effect in comparison with that induced by EPI alone (Scheme 1B). The released antigens and DAMPs after ICD could function as a nanovaccine to enhance the antigenicity and adjuvanticity, potentiating DCs maturation and cytotoxic T lymphocytes (CTLs) infiltration to activate the tumor immune microenvironment (Scheme 1C). In this context, an enhanced antitumor chemoimmunotherapeutic efficacy could be achieved in a murine 4T1 model. Therefore, the self-amplified biomimetic nanosystem could induce a potent ICD effect and activate the tumor immune microenvironment, boosting the therapeutic efficacy of anti-PD-L1 antibody against tough cancers of TNBC.

2. Materials and methods

2.1. Materials

Zinc acetate, 2-methylimidazole (2-MI) and hemin were purchased from Aladdin Biochemical Technology Co. Ltd. (Shanghai, China). Gox and 2′,7′-Dichlorodihydrofluorescein diacetate (DCFH-DA) were obtained from Sigma-Aldrich (Shanghai, China). 4′,6-diamidino-2-phenylindole (DAPI) and GSH detection kit were purchased from Solarbio (Beijing, China). Cell membrane fluorescence probe (Dio), an ATP detection kit, BCA protein assay kit and live, dead viability assay kit and Protease inhibitor cocktail (100 ×) were purchased from Beyotime Biotechnology (Shanghai, China). Annexin V apoptosis kit was obtained from Yeason (Shanghai, China). Antibodies against CD45, CD3, CD8, CD4, CD11c, CD80, CD86, IFN-γ for flow cytometry were obtained from BioLegend (San Diego, California, USA). ELISA kits for analysis of cytokines were purchased from Thermo Fisher (Waltham, USA). Anti-mouse-PD-L1 antibody (BE0101) were purchased from Bio X Cell (Lebanon, USA). All other chemical reagents were analytically pure and used directly as received.

2.2. Cell lines and animals

The 4T1 murine breast cancer cell line and RAW 264.7 cell line were obtained from Chinese Academy of Science Cell Bank for Type Culture Collection (Shanghai, China). 4T1 cells were cultured in the PRMI 1640 medium (Hyclone, USA) supplemented with 10% fetal bovine serum (FBS) (Gibco, USA) and 1% penicillin-streptomycin (Hyclone, USA), while Raw 264.7 cells were cultured in DMEM-high glucose medium (Hyclone, USA) with 10% FBS (Gibco, USA) and 1% penicillin-streptomycin (Hyclone, USA) in an incubator with 5% CO_2 at 37 °C. Female mice of 4–6 weeks (18.0 ± 2.0 g) were purchased from Chengdu Dashuo Experimental Animals Co. Ltd. These animals were fed at a specific pathogen free (SPF) standard condition on a 12 h light/12 h dark cycle. All animal experiments were carried out according to the guidelines of the Ethics Committee of West China Hospital, Sichuan University (No. 2018148A and 2018150A).

2.3. Synthesis of ZIF-8 and encapsulation of EPI

(1) Synthesis of ZIF-8: ZIF-8 was synthesized by the "one-pot" method in a previous report with modification [31]. The concentrations of zinc acetate and the 2-MI solution were selected by comparing the dynamic light scattering (DLS) size of the ZIF-8 particles shown in Table 1 (supporting information). A zinc acetate aqueous solution (0.25 mL, 200 mg/mL) was dropwise added into 2.5 mL of 2-MI aqueous solution (200 mg/mL). The mixture was stirred at room temperature for 30 min, and then centrifuged (13000 g, 30 min) to obtain white precipitates (ZIF-8). (2) Encapsulation of EPI: An EPI stock solution (100 μL, 20 mg/mL) was mixed with the zinc acetate solution and the mixture was dropwise added into the 2-MI solution. The same procedure as (1) was repeated to obtain precipitates (EZ). (3) Encapsulation of Gox and hemin: A Gox aqueous solution (50 μL, 20 mg/mL) and hemin (50 μL,10 mg/mL) were mixed with the 2-MI solution. The zinc acetate solution was dropwise added to the prepared mixture. The same procedure as (1) was repeated to obtain precipitates (GHZ). (4) Encapsulation of EPI, Gox and hemin: An EPI stock solution was added to the zinc acetate solution. A Gox aqueous solution and hemin were mixed with the 2-MI solution. The two mixtures were mixed under stirring. The same procedure as (1) was repeated to obtain precipitates (EHGZ).

The loading amounts of EPI and hemin in nanoparticles were determined by fluorescence and UV–vis absorption spectroscopy, respectively. The drug loading efficiency (LE) was calculated by the equation: $LE = (m_t\text{-}m_f)/m_t$, where m_t is the total amount of EPI or hemin initially added and m_f is its amount in the supernatant.

2.4. Collection of tumor cell membrane and coating of membrane onto NPs

4T1 cell membranes were collected via a similar procedure according to the literature [29]. Briefly, cells were collected by scraping after they reached confluence. The collected cells were washed in cold PBS three times, and then in a buffer solution of 30×10^{-3} M Tris-HCL (pH = 7.0) with 0.0759 M sucrose and 0.225 M D-mannitol three times. Cells were dispersed in a cocktail solution (1 ×) containing phosphatase inhibitor and protease inhibitor and they were mechanically disrupted via an ultrasonic probe at a power of 35% (3 s on and 5 s off, 20 times) in an ice bath. The solution was centrifuged at 10000 g, 4 °C for 35 min to remove organelles. The collected supernatants were centrifuged at 150000 g, 4 °C for 35 min to obtain the cell membrane. To induce CRT expression on the tumor cell membrane, 4T1 tumor cells were pre-treated with EPI overnight. The above membrane collection process was repeated for those pre-treated cells to obtain the cell membrane with over-expressed CRT. The protein content on the cell membrane was measured via a BCA protein assay kit according to the manufacturer's instruction.

To prepare biomimetic nanoparticles, mEHGZ, the EHGZ nanoparticles were dispersed in DI water. The cell membrane solution with an equal mass of the nanoparticles was added to the nanoparticle solution under stirring. The mixture was disrupted using an ultrasonic probe at a power of 45% (3 s on and 5 s off, 15 times), and the coated nanoparticles were obtained after centrifugation (4 °C, 15000 g, 45 min).

2.5. Nanoscale flow cytometry to determine the coating efficiency

4T1 cells were stained with Dio for 15 min to obtain the Dio-staining cell membrane. The Dio-staining cell membrane was collected to coat EHGZ nanoparticles using the same procedure detailed in 2.4. The membrane-coated nanoparticles were subjected to flow cytometry analysis according to the protocol of nanoscale flow cytometry. The coating efficiency was determined from the ratio of Dio^+-EPI^+ nanoparticles to the total number of nanoparticles.

2.6. Identification of membrane-associated proteins

The membrane-associated proteins were confirmed via coomassie blue staining and western blotting. The cell membrane collected from 4T1 cells, the cell membrane with over-expressed CRT, or mEHGZ at an equivalent 20 μg of proteins was loaded into each well of a 12% Tris/glycine SDS-polyacrylamide gel. For coomassie blue staining imaging, gelatin was stained in a coomassie blue fast staining solution for 30 min, and exposed in a gel imaging system. To execute western blotting analysis, proteins were transferred to polyvinylidene fluoride membranes. They were blocked in 5% BSA solution for 1 h, and incubated with an CRT/Na^+-K^+ ATPase antibody overnight at 4 °C and an anti-HRP rabbit antibody for 2 h. The proteins were visualized in an imaging system (Bio Rad Image system).

2.7. Cell viability and apoptosis analysis

The *in vitro* cytotoxicity was evaluated via the CCK-8 assay. 4T1 cells were seeded in 96-well plates for 24 h, and the solutions of EPI, EZ, GHZ, EHGZ or mEHGZ were added at an equal EPI amount of 1.6, 1.4, 1.2, 1.0, 0.8, 0.6, 0.4, 0.2 and 0.1 μg/mL. A PBS solution was used as a control. Cells were incubated with these solutions for 24 h. The CCK-8 kit in the cell culture medium was added to cells and then incubated for 2 h, the OD_{450} value was read to calculate the relative cell viability by normalizing the OD_{450} readings of samples by that of the control. Live-dead cell staining was also carried out for direct visualization of the cell viability. 4T1 cells were seeded in 24-well glass plates, and cells were treated with EPI, EZ, GHZ, EHGZ, or mEHGZ at the equivalent EPI concentration of 1 μg/mL for 12 h. Cells treated with PBS were used as a control. Viable cells were stained with calcein as green (λ_{ex} = 494 nm, λ_{em} = 517 nm),

while dead cells with DAPI as blue ($\lambda_{ex} = 340$ nm, $\lambda_{em} = 488$ nm) under a fluorescence microscope.

The apoptosis of 4T1 cells was determined via an Annexin V apoptosis kit via flow cytometry (BD). Briefly, 4T1 cells were seeded in 6-well plates (5×10^5 cells) for 24 h, subsequently, they were cultured with EPI, EZ, GHZ, EHGZ, or mEHGZ at the same EPI concentration of 1 μg/mL for 12 h. The treated cells were collected (4 °C, 1000 rpm, 3 min) and suspended in the Annexin V binding buffer, stained and washed according to the supplier's protocol.

2.8. Cellular uptake

4T1 cells were seeded in 12-well plates for 24 h and they were then cultured in the medium containing EPI, EZ, GHZ, EHGZ, or mEHGZ at an equivalent EPI concentration of 2 μg/mL for 2 h. They were centrifuged (4 °C, 1000 rpm, 3 min) and washed with PBS for flow cytometry analysis. To visualize the cellular uptake process, cells were seeded in confocal glass dishes and they were subjected to the same treatment. These cells were washed and fixed with 4% paraformaldehyde, and their nuclei were stained with DAPI. The cells were visualized under a confocal scanning laser microscope (CLSM).

2.9. Intracellular •OH generation

A ROS probe, 2′, 7′-dichlorofluorescin diacetate (DCFH-DA) ($\lambda_{ex} =$ 488 nm, $\lambda_{em} = 525$ nm), was used to detect *in vitro* free radicals generation. 4T1 cells were seeded in 24-well plates for 24 h at 37 °C. EPI, EZ, GHZ, EHGZ, or mEHGZ at an equivalent EPI dose of 1.0 μg/mL was added to incubate for 12 h. 1 μM of the DCFH-DA solution was incubated with the treated cell for 30 min. Cells were collected and washed with PBS for flow cytometry analysis. The cell nucleus was stained with DAPI for visualization.

2.10. Intracellular glutathione (GSH) detection

To detect the *in vitro* GSH level, 4T1 cells were seeded in 6-well plates and incubated at 37 °C with 5% CO_2 for 24 h. They were treated with EPI, EZ, GHZ, EHGZ, or mEHGZ at an equivalent EPI dose of 1.0 μg/mL for 12 h. Cells treated with PBS were used as a control. The cells were collected for detecting the intracellular GSH content according to the GSH detection kit's instruction.

2.11. Induction of immunologic cell death (ICD)

To confirm ICD of 4T1 tumor cells after treatment with nanoparticles, CRT and HMGB1 were detected via immunofluorescence and the released ATP was analyzed via ATP detection kit. Briefly, 4T1 cells were seeded on a 24-well glass bottom cell culture dish at a density of 1×10^5 per well. After 24 h incubation, EPI, EZ, GHZ, EHGZ, or mEHGZ at an equivalent EPI dose of 2.0 μg/mL was added into the well and incubated with cells for 4 h. The cells were washed with PBS twice and fixed with 4% paraformaldehyde. They were incubated with 5% BSA for 30 min, anti-CRT antibody or anti-HMGB1 antibody overnight in 4 °C and APC-conjugated secondary antibody for 2 h. The nuclei were stained with DAPI at room temperature for 8 min. The fluorescence signal of CRT and HMGB1 was detected via a confocal scanning laser microscope ($\lambda_{ex} = 633$ nm, $\lambda_{em} = 660$ nm). For ATP detection, 1×10^5 4T1 cells were seeded on a 6-well plate and cultured with EPI, EZ, GHZ, EHGZ, or mEHGZ. The supernatants were collected, and the extracellular ATP content was measured with an ATP assay kit according to the manufacturer's instruction.

2.12. Immune activation effect of CRT-over expressed coated nanosystem

RAW 264.7 cells and bone marrow-derived dendritic cells (BMDCs) were used to evaluate the immune response activated by the collected cell membrane. BMDCs were generated from bone marrow mesenchymal stem cells according to the report [32]. Briefly, BMDCs were obtained from the femurs and tibiae of male C57BL/6 mice at 4–6 weeks. The suspensions were dispersed in a red blood cell lysis buffer and centrifuged to obtain precipitates. The precipitates were incubated in the RPMI 1640 medium containing 10% FBS and 20 ng/mL GM-CSF for 5 days to yield BMDCs. RWA264.7 cells and BMDCs were seeded in 24-well plates and cultured with the cell membrane or the CRT over-expressed cell membranes at the concentration of 0.4, 0.2, 0.1 or 0.05 mg/mL for 12 h. These cells were stained with anti-mouse11c/80 antibodies for flow cytometry analysis. After the obtained BMDCs were cultured in a lower chamber of a Transwell system, 4T1 cells treated with EPI, EZ, GHZ, EHGZ, or mEHGZ at an equivalent EPI dose of 1 μg/mL for 12 h were added into the upper chamber. After 24 h incubation, the BMDCs were collected and stained with anti-11c, anti-80 antibodies for flow cytometry analysis the ratio of $CD11c^+CD80^+$ BMDC cells.

2.13. In vivo activated immune cells analysis

To examine potent immune responses in 4T1-bearing mice induced by mEHGZ, the percentages of $CD8^+$ T cells and mature DCs were measured via a flow cytometer. The mice were euthanized two days after the last treatment with EPI, EZ, GHZ, EHGZ, mEHGZ, anti-PD-L1 antibody, and mEHGZ + anti-PD-L1 antibody at an equivalent EPI dose of 3 mg/kg, and/or anti-PD-L1 antibody (BE01001) dose of 100 μg. The tumor, lymph nodes, and spleen were harvested. The tumor was cut into pieces and centrifuged to obtain the supernatant for ELISA analysis of IFN-γ, TNF-α, and IL-6. The pellets were digested in a solution containing hyaluronidase/collagenase IV and Deoxyribonuclease I in a shaker at 37 °C for 30 min to generate a single cell suspension. The cells were filtered through a 70 μm filter and dispersed in 5% BSA to block the non-specific Fc fragment. The isolated cells were stained with fluorochrome-conjugated antibodies: anti-mouse CD45, anti-mouse CD3, anti-mouse CD4, anti-mouse CD8, anti-mouse IFN-γ, anti-mouse CD11c, anti-mouse CD80 or anti-mouse CD86 for flow cytometry analysis. Analysis of $CD8^+$ T cells in the spleen and lymph nodes were executed with a similar procedure as that for the tumor tissue.

2.14. Anti-tumor studies in vivo

To establish a 4T1 subcutaneous tumor model, 5×10^5 4T1 cells were subcutaneously injected into the right lower back of mice. The tumor volume (V) was monitored and calculated from the equation: $V = ab^2/2$, where a and b are the length and width of the tumor. When the tumor volume reached about 50–75 mm^3, the mice were randomly divided into eight groups (n = 5 in each group) and they were treated with saline, free EPI, EZ, GHZ, EHGZ, mEHGZ, anti-PD-L1 antibody, and mEHGZ + anti-PD-L1 antibody. These formulations were intratumoral injection at an equivalent EPI dose of 3 mg/kg. An anti-PD-L1 antibody (BE01001) at a dose of 100 μg was intraperitoneally injected on the following day. This treatment cycle was repeated three times every two days. The tumor volume and the body weight were recorded every other day. At the end of the treatment, mice were sacrificed to collect tumors and major organs for H&E, TUNEL, KI67 staining, and immunohistochemistry analysis.

2.15. Statistical analysis

All quantitative values were presented as means ± SD. Student's t-test was used for the statistical analysis of differences between two groups, and statistical significance was set at a 95% confidence level for all tests, *$p < 0.05$, **$p < 0.01$, ***$p < 0.001$ and ****$p < 0.0001$.

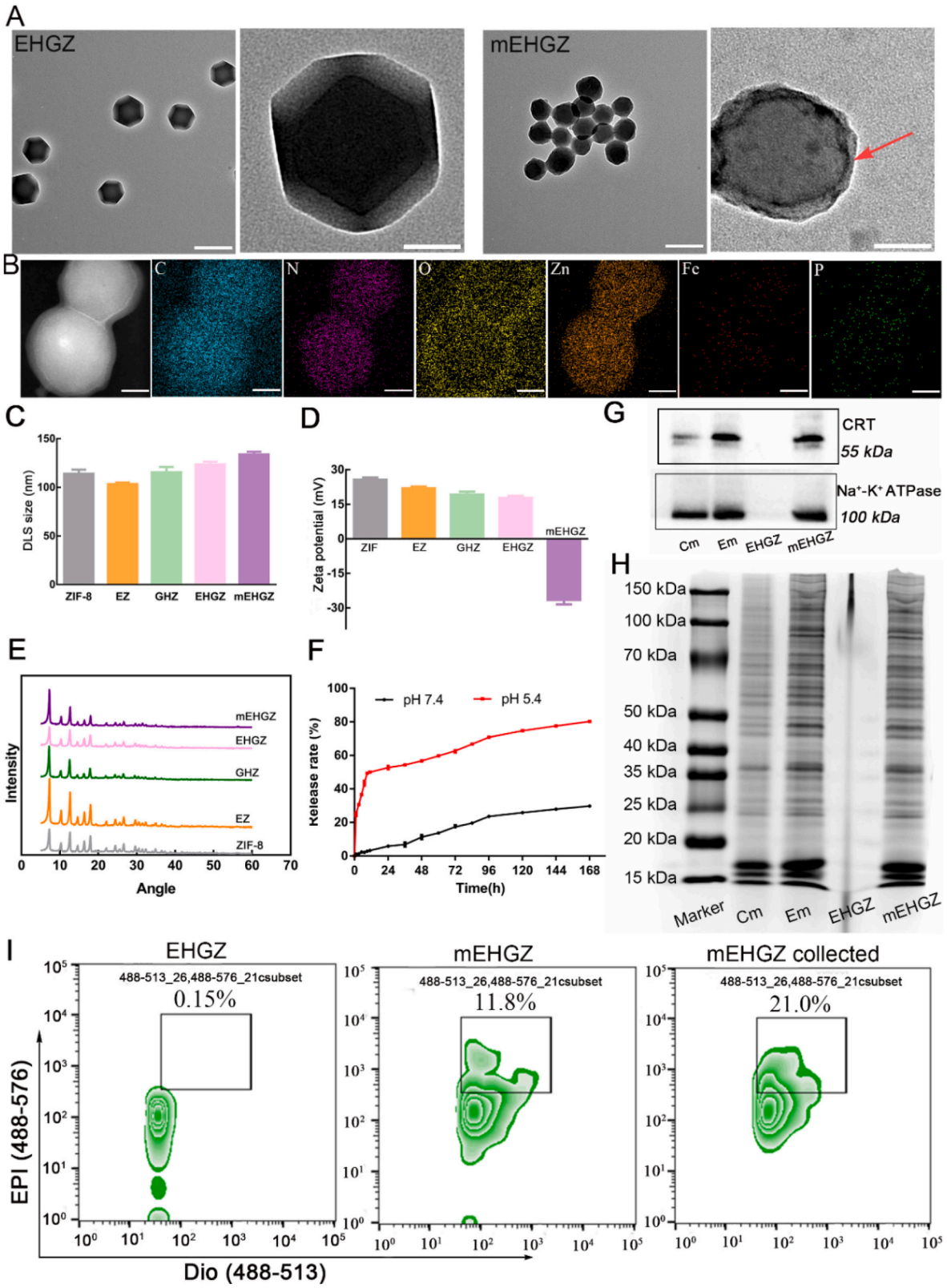

Fig. 1. Preparation and characterizations of EHGZ after encapsulation of EPI, Gox and hemin into ZIF-8 nanoparticles and mEHGZ after coating of the drug-loaded nanoparticles with tumor cell membrane. A) TEM images of EHGZ and mEHGZ, scale bar = 100 nm. B) EDS elemental mapping images of mEHGZ for element C, N, O, Zn, Fe and P, scale bar = 30 nm. C-D) DLS sizes and zeta potentials of ZIF-8, EZ, GHZ, EHGZ, and mEHGZ. E) XRD patterns of ZIF-8, EZ, GHZ, EHGZ, and mEHGZ. F) The release profiles of EPI from EHGZ at pH of 7.4 and 5.4. G-H) Western blotting and coomassie blue staining images of cell membrane (Cm), EPI-treated membrane (Em), EHGZ and mEHGZ. I) Flow Nano Analyzer results to determine the coating efficiency of the cell membrane onto the drug-loaded ZIF-8 nanoparticles.

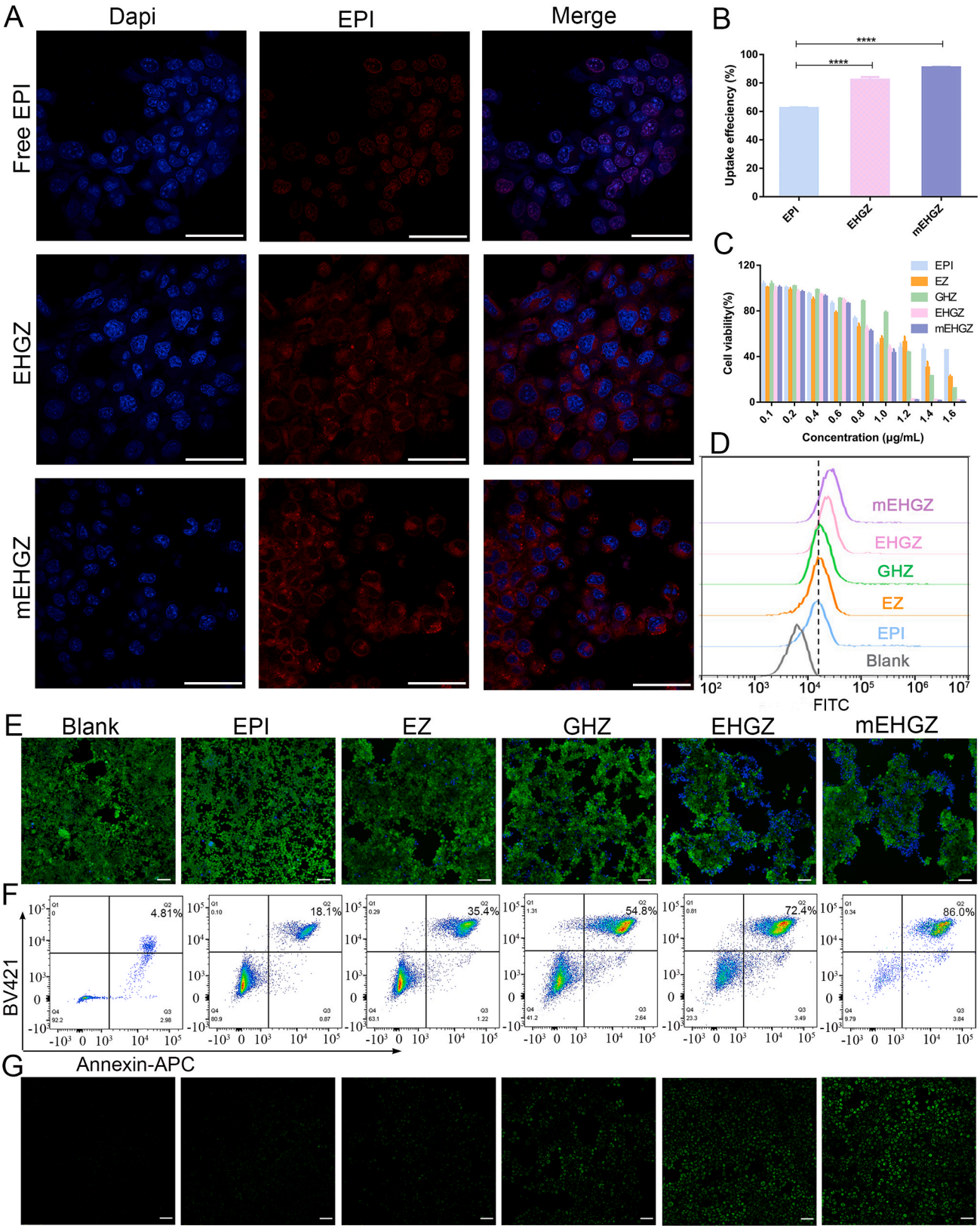

Fig. 2. Intracellular uptake, cytotoxicity and ROS generation. A) CLSM images of cells treated with EPI, EHGZ, and mEHGZ after incubation of them with 4T1 cells for 2 h (blue: cell nuclei; red: EPI; scale bar = 20 μm). B) Flow cytometry analysis of the uptake efficiency of EPI, EHGZ and mEHGZ by 4T1 cells. Cytotoxicity of EPI, EZ, GHZ, EHGZ, and mEHGZ at different concentrations against 4T1 cells via the CCK-8 assay C), visualization by live and dead stained kit E) (Scale bar = 100 μm, green: live cells; blue: dead cells); Flow cytometry analysis of live and dead staining 4T1 cells via Annexin V-apoptotic assay kit F). Intracellular ROS generation after treatment with EPI, EZ, GHZ, EHGZ, and mEHGZ was detected Flow cytometry quantification D) and fluorescence microscope G). *$p < 0.05$, **$p < 0.01$, ***$p < 0.001$, ****$p < 0.0001$.

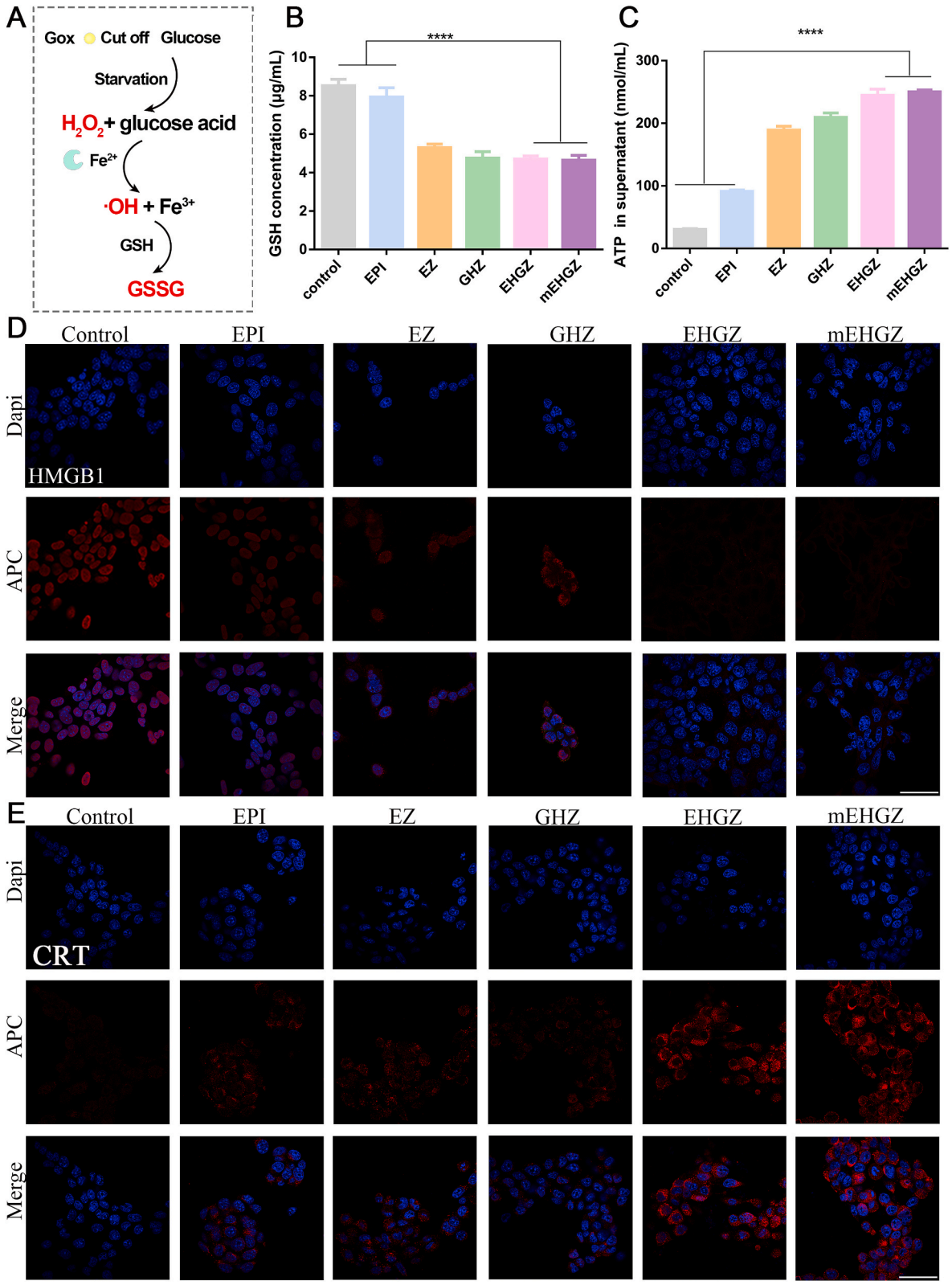

Fig. 3. *In vitro* ICD effect induced by the self-amplified nanosystem. A) Schematic diagram of a cascade process to generate cytotoxic ·OH and deplete intracellular GSH. B) GSH content in 4T1 cells after co-culture with EPI, EZ, GHZ, EHGZ, and mEHGZ for 12 h. C) ATP released in the supernatant after treatment with different preparations. D-E) CLSM images for HMGB1 distribution and CRT exposure in 4T1 cells after treatment of them with EPI, EZ, GHZ, EHGZ, and mEHGZ at an EPI concentration of 2 μg/mL for 4 h (blue: cell nuclei; red: HMGB1 or CRT; scale bar = 50 μm). *$p < 0.05$, **$p < 0.01$, ***$p < 0.001$, ****$p < 0.0001$.

3. Results and discussion

3.1. Synthesis and characterizations of biomimetic mEHGZ nanoparticles

The process for self-assembly of nanoscale metal-organic frameworks (nMOFs) from Zn^{2+} and 2-MI, encapsulation of EPI, Gox and hemin into nMOFs, and coating of the nanoparticles with tumor cell membrane is presented in Scheme 1. The ZIF-8 nanoparticles with porosity display an excellent encapsulation ability, and the EPI and hemin entrapment efficiency in ZIF-8 nanoparticles are 81.42% and 84.7%, respectively. (Figs. S1 and S2). Transmission electron microscopy (TEM) images (Fig. 1A) show that these nanoparticles display a regular tetrahedral shape with a diameter size of 110 nm. The thickness of the outermost layer composed of the tumor cell membrane is about 10 nm. The hydrodynamic size of EHGZ via DLS is 123.66 ± 2.83 nm. After coating the cell membrane onto EHGZ, the DLS size increases to 133.92 ± 2.93 nm (Fig. 1C), which is consistent with the TEM result. Furthermore, the surface charge after coating changes from 17.77 ± 0.95 mV to – 26.47 ± 1.98 mV (Fig. 1D), which indicates successful coating of the cell membrane onto EHGZ nanoparticles. Powder X-ray diffraction (XRD) patterns (Fig. 1E) of EZ, GHZ, EHGZ, mEHGZ are identical to those of blank ZIF-8 nanoparticles, which suggests that the cargo in the cavity of ZIF-8 nanoparticles and the sonication process for facilitating the coating process have no impact on the crystallinity of ZIF-8. Fourier transform infrared (FTIR) spectra support EPI, Gox and hemin are encapsulated in ZIF-8 nanoparticles (Fig. S3). It has been reported that ZIF-8 nanoparticles degrade at a low pH and they are a natural pH-responsive nanocarrier to release the loaded drug in a controlled manner [33]. The *in vitro* release profile for EPI from ZIF-8 nanoparticles confirms that these nanoparticles are responsive to a low pH. The released amount of EPI in a buffer at pH 5.4 is about ten times higher than that in a buffer at pH 7.4 (Fig. 1F). A similar release result for mEHGZ is observed, and the drug release rate at pH 5.4 is quicker than that at pH 7.4 (Fig. S4). The sustained drug release from mEHGZ lasts up to 168 h, and at this time point the drug carrier is observed to be cleared through the liver metabolism. The detailed information of the metabolism process of ZIF-8 nanoparticles is shown in Table 2 (supporting information). Furthermore, there are negligible changes in the hydrodynamic size distribution and polydispersion index (PDI) of EHGZ and mEHGZ in PBS for 72 h (Fig. S5), suggesting these nanoparticles are favorably stable.

After tumor cells are pre-treated with a chemotherapeutic drug like EPI, ICD may be triggered in these cells and CRT could migrate from the ER to the cell membrane. The collected cell membrane for coating EHGZ nanoparticles would evoke the immune system because CRT may bind to CD91 on APCs [34]. After 4T1 tumor cells were treated with 2 μg/mL EPI for 12 h, significantly CRT is seen to relocate on the tumor cell membrane (Fig. 1G and Fig. S6) according to western blot analysis. The membrane-associated protein profiles in the coomassie blue staining images of the CRT over-expressed membrane are identical to those of mEHGZ (Fig. 1H), suggesting the membrane proteins are intact retained on the mEHGZ nanoparticles. Furthermore, the EDS mapping supports that the membrane is successfully coated onto the EHGZ nanoparticles since the P element is the main component of cell membrane proteins (Fig. 1B). As shown in Fig. S7, after the cell membrane was stained with Dio, it emits green fluorescence ($\lambda_{ex} = 484$ nm, and $\lambda_{em} = 501$ nm). The ratio of the cell membrane coated onto the nanoparticles was evaluated via nanoscale flow cytometry. According to Fig. 1I, the membrane coating efficiency is 11.8%, while it raises nearly two folds to 21.0% after centrifugal collection. The coating efficiency is similar to that reported by *Liu* et al. [35]. However, the membrane coating efficiency is quite low via the sonication approach. The membrane coating method need to be optimized for a high coating efficiency to maximize the use of the tumor cell membrane.

3.2. In vitro cytotoxicity and cell uptake of mEHGZ

It is reported that the proteins on the cancer cell membrane play an important role in homologous recognition [36,37], therefore cancer cell membrane-camouflaged nanoparticles may have the potential to achieve specific targeting towards the same cancer cells. As shown in the CLSM images (Fig. 2A), after incubation of free EPI, EHGZ, and mEHGZ with 4T1 cells for 2 h, the red fluorescence intensity in 4T1 cells incubated with mEHGZ is much stronger than that of the cells treated with free EPI, suggesting that mEHGZ promotes cellular uptake in 4T1 cells. Furthermore, the cellular uptake efficiency is 62.33%, 82.4% and 91.04% for free EPI, EHGZ, and mEHGZ, respectively (Fig. 2B), which is coincident with CLSM images. The EHGZ nanoparticles display an enhanced uptake efficiency since these positively charged nanoparticles may interact with negatively charged tumor cell membrane. mEHGZ nanoparticles outperform free EPI and EHGZ in their cellular uptake since the coated cell membrane may promote homologous and rapid fusion with the target tumor cells. Furthermore, the uptake efficiency of mEHGZ by 293T cells, HUVEC and RAW264.7 cells is 4.71, 3.49, 4.76 folds lower than that by 4T1 cells (Fig. S8), which suggests that the coated 4T1 cell membrane could medicate homotypic target ability.

The CCK-8 assay was used to evaluate the cell viability of 4T1 cells after incubation with EHGZ and mEHGZ nanoparticles. As shown in Fig. 2C, when EPI, Gox and hemin were loaded into ZIF-8 nanoparticles, the lowest cell viability is observed in 4T1 cells, indicating that Gox may exert a starvation effect on tumor cells and hemin promotes the Fenton reaction and GSH depletion, synergistically reducing the cell viability. mEHGZ displays negligible cytotoxicity against APCs such as RAW264.7 and DC2.4 cells (Fig. S9), which supports that mEHGZ could not influence the viability of APCs. Furthermore, cytotoxicity induced by the self-amplified delivery system was confirmed with a live and dead viability assay kit. Exposure to EHGZ and mEHGZ leads to the highest ratio of dead cells stained by DAPI compared with other groups (Fig. 2E). The 4T1 cells death mechanism after different treatments was studied via an Annexin V-FITC apoptosis kit and a flow cytometer. According to Fig. 2F, the percentage in the Q2 of the flow cytometry for late apoptosis is 18.1%, 35.4%, 54.8%, 72.4%, and 86.0% after treatment with EPI, EZ, GHZ, EHGZ, and mEHGZ, respectively. mEHGZ nanoparticles have the highest potency in inducing apoptosis of 4T1 cells in comparison with other groups at an equal dose of EPI. These consistent results from the CCK-8 assay, live and dead staining and the apoptosis assay suggest that mEHGZ could be an excellent therapeutic nanomedicine against 4T1 tumor cells.

3.3. ROS generation and depletion of GSH by mEHGZ nanoparticles

Intracellularly generated ROS, a competent inducer for ICD, perturb the balance between protein folding load and capacity, resulting in an elevated ER stress [38]. Compared to normal cells, GSH, a powerful reductant, is over-expressed in tumor cells to maintain the oxidation-reduction homeostasis in a tumor microenvironment [39,40]. We designed a cascade reaction to promote ROS generation and deplete intracellular GSH to strengthen the ER stress that could amplify the ICD effect. After EPI, Gox and hemin were released from the porous ZIF-8 nanoparticles, Gox oxidizes glucose to hydrogen peroxide, and Fe^{2+} in hemin reacts with hydrogen peroxide to generate cytotoxic ·OH and Fe^{3+}. The generated Fe^{3+} oxidizes GSH, leading to an up-regulated ROS level and a depleted level of GSH, thus breaking the oxidation-reduction balance (Fig. 3A). A ROS probe, DCFH-DA, is non-fluorescent, but it can be oxidized by intracellular ROS to produce green fluorescent 2′, 7′-dichlorofluorescein (DCF). Thus, the probe was used to evaluate the ROS level inside tumor cells via flow cytometry (Fig. 2D) and fluorescence microscopy. It can be seen that the fluorescence intensity in cells treated with EHGZ or mEHGZ is remarkably strong, while weak fluorescence is seen in cells treated with EZ or GHZ nanoparticles, which

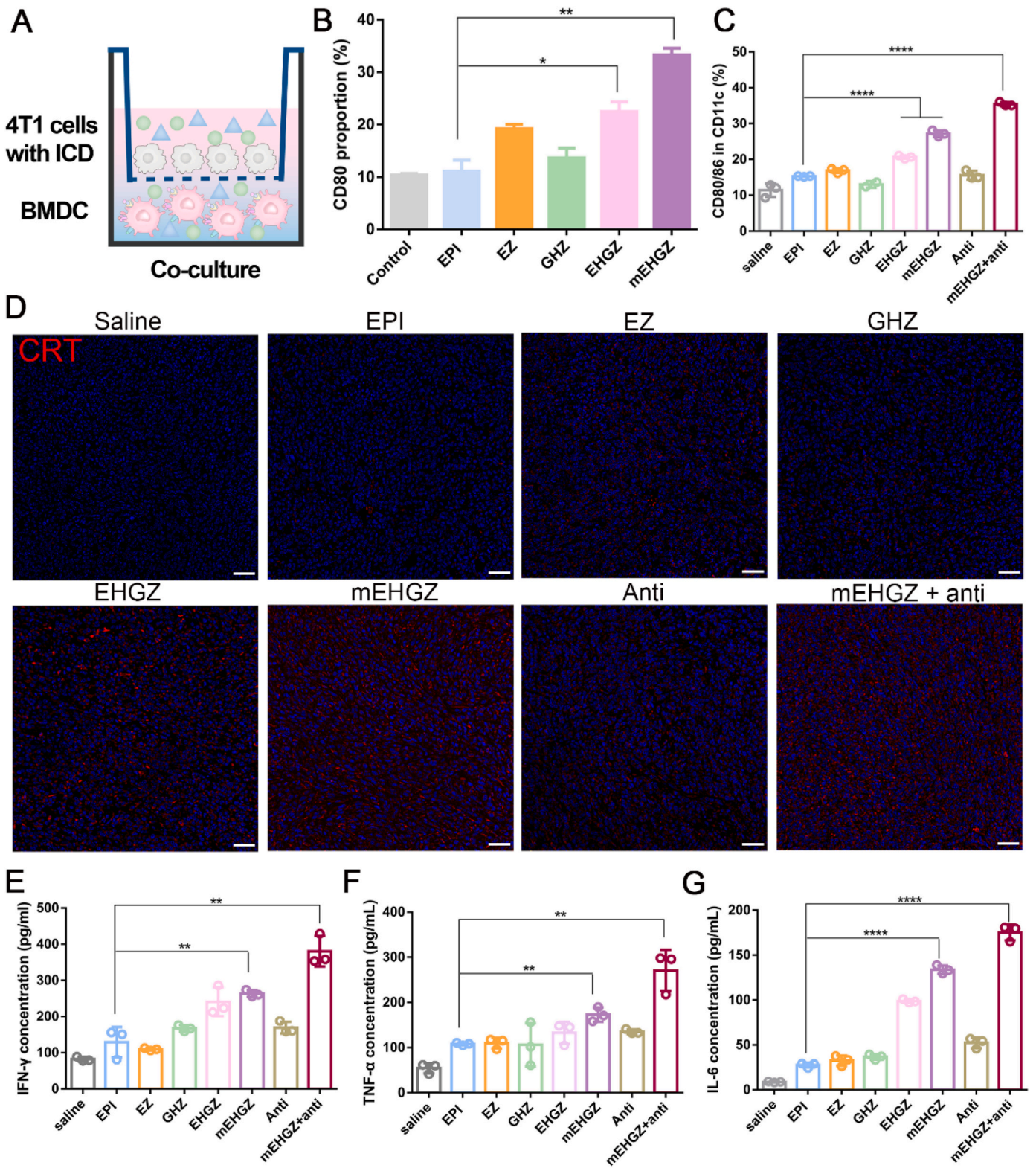

Fig. 4. DCs maturation and cytokines secretion induced by the cell membrane-coated biomimetic nanoparticles. A) Schematic illustration of co-culture of 4T1 cells and BMDCs after 4T1 cells were incubated with EPI, EZ, GHZ, EHGZ, and mEHGZ at an EPI concentration of 1 μg/mL for 12 h. B) The percentage of mature BMDCs ($CD80^+CD11c^+$) in the co-culture experiment measured by flow cytometry. C) The percentage of $CD11C^+CD80^+CD86^+$ cells in the tumor tissue after treatment with EPI, EZ, GHZ, EHGZ, mEHGZ, anti-PD-L1 antibody, and mEHGZ + anti-PD-L1 antibody at an EPI dose of 3 mg/kg and 100 μg anti-PD-L1 antibody. D) CLSM images of CRT exposure on the tumor cell membrane in the tumor tissue after treatment with EPI, EZ, GHZ, EHGZ, mEHGZ, anti-PD-L1 antibody, and mEHGZ + anti-PD-L1 antibody three times. (blue: cell nuclei; red: CRT; scale bar = 100 μm). E-G) The concentration of IFN-γ, TNF-α, and IL-6 in the supernatant extracted from the tumor tissue after various treatments. $^*p < 0.05$, $^{**}p < 0.01$, $^{***}p < 0.001$, $^{****}p < 0.0001$.

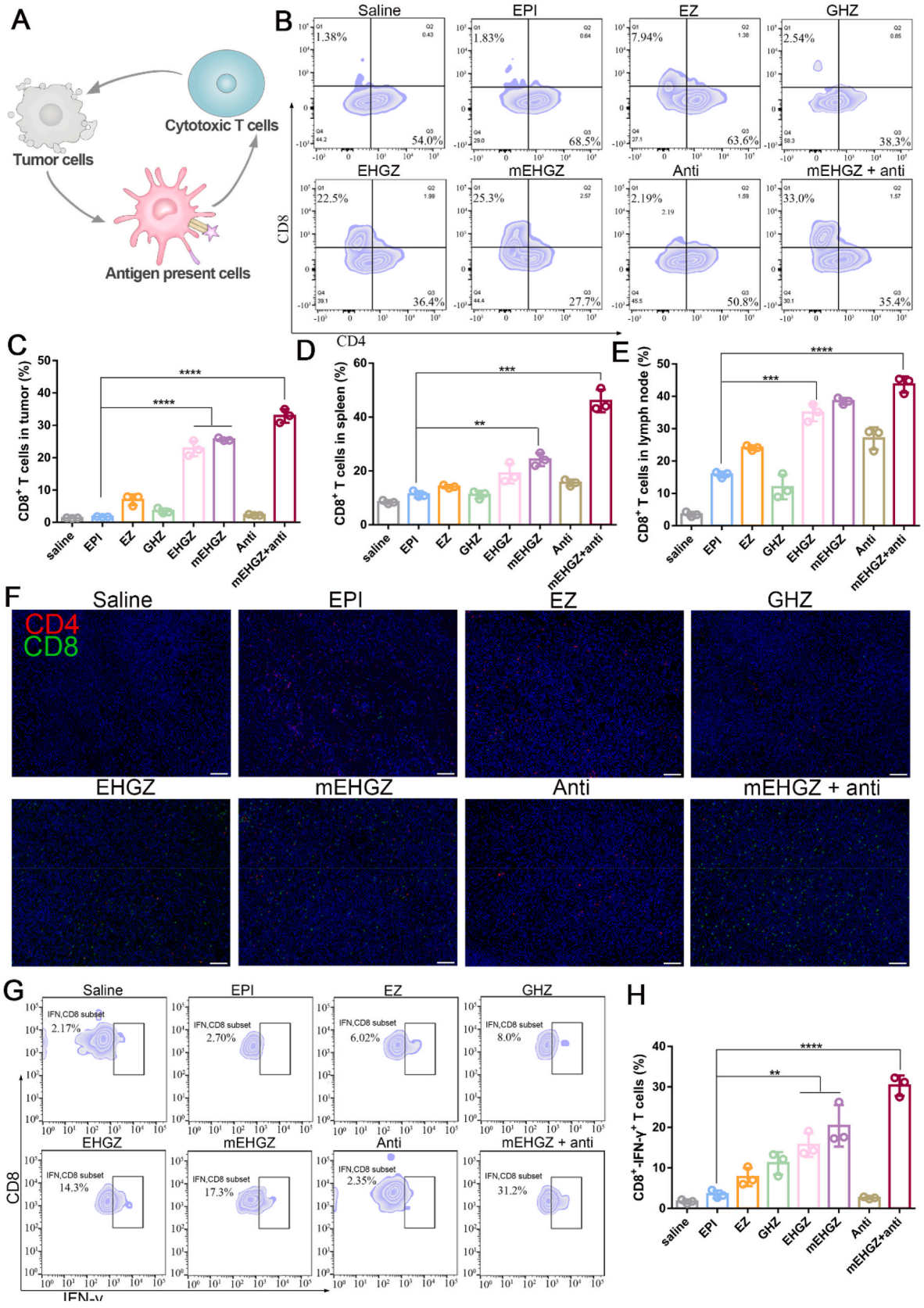

Fig. 5. $CD8^+$ T cell infiltration into the tumor tissue after treatment with EPI, EZ, GHZ, EHGZ, mEHGZ, anti-PD-L1 antibody, and mEHGZ + anti-PD-L1 antibody at an EPI dose of 3 mg/kg or an antibody dose of 100 μg for three time every two days to activate the immune microenvironment. A) Schematic illustration of the released antigens and DAMPs triggered by ICD to reverse an immunosuppressive microenvironment to an immunosupportive one. B–C) The proportion of $CD8^+$ T cells in the tumor tissue after different treatments. D-E) Quantification of $CD8^+$ T cells in the spleen and lymph nodes via flow cytometry. F) Immunofluorescence slices indicating $CD8^+$ T cells infiltration into the tumor tissue. (blue: nuclei; red: $CD4^+$ T cells; green: $CD8^+$ T cells; scale bar = 100 μm). G) Flow cytometric analysis of IFN-γ $CD8^+$ T cells in the tumor tissue. *$p < 0.05$, **$p < 0.01$, ***$p < 0.001$, ****$p < 0.0001$.

indicate that treatment with EPI combined with Gox and hemin could generate a high level of ROS in tumor cells (Fig. 2G). The ROS generation was detected via mice ROS ELISA detection kit in the tumor tissue. The ROS content increases from 43.25 IU/mL to 104.62 IU/mL in the tumor tissue after treatment with EPI or mEHGZ (Fig. S10). Furthermore, the GSH level in 4T1 cells after treatment with mEHGZ reduces 1.7 folds compared to the EPI-treated group (Fig. 3B) and a 2.2-fold reduction in the GSH level is seen in the tumor tissue after treatment with mEHGZ (Fig. S11), confirming the self-amplified nanoparticles could reduce the intracellular GSH level.

3.4. In vitro ICD induced by nanoparticles

CRT exposure, HMGB1 transfer and ATP release are the hallmarks of ICD. As shown in Fig. 3C, the concentration of ATP in the supernatant of cells after treatment with mEHGZ is 250.30 μM, in comparison with 91.40 μM in the group treated with EPI. An 2.74-fold increase in the released ATP indicates the amplified ER stress could strengthen the ICD effect compared to a single chemotherapeutic drug EPI. Meanwhile, the ATP content in tumor tissue is 48.29 nM and 103.59 nM in the tumor tissue after treatment with EPI and mEHGZ, respectively (Fig. S12). The majority of HMGB1 is located in the cell nucleus after PBS treatment, but it gradually transfers from the nucleus to the cytoplasm in the groups treated with EPI, EZ, GHZ, or EHGZ nanoparticles. Strikingly, the vast majority of HMGB1 is found in the cytoplasm in the cells treated with mEHGZ (Fig. 3D). CRT exposure on the cell membrane triggers DCs to swallow the released antigens, which invokes the tumor-immunity cycle. CLSM images in Fig. 3E show that cells treated with EPI alone leads to a negligible level of CRT exposure, while the strongest red fluorescence intensity is seen in the mEHGZ-treated group, suggesting that mEHGZ can strongly induce CRT transportation from the ER to the cell membrane. These DAMPs results suggest a potent ICD effect is induced by the self-amplified delivery system.

3.5. Cell membrane with overexpressed CRT as an immune adjuvant

CRT exposure on the cell membrane activates DCs to present and process antigens, acting as a promising immune adjuvant [41,42]. The function of the cell membranes with over-expressed CRT was evaluated after culture of the cell membrane with BMDCs and RAW 264.7 cells. The proportion of matured cells is found to be positively correlated with the concentration of the cell membrane (Fig. S13 and Fig. S14). The ratio of $CD80^+$ BMDCs is 51.03% when they were co-cultured with 0.2 mg/mL of the CRT-overexpressed cell membrane, while it is 34.8% after treatment with the normal 4T1 cell membrane at the same concentration (Fig. S13). The membranes with over-expressed CRT at a concentration of 0.2 mg/mL is able to induce 56.83% of RAW 264.7 cells to become mature, while only 27.17% is seen after treatment with the normal cell membrane at the same concentration (Fig. S14), indicating that CRT acts an important player to promote APCs maturation.

To mimic the *in vivo* ICD effect, BMDCs were inoculated in the lower chamber of a Transwell chamber and 4T1 cells were placed in the upper chamber after they were treated with nanoparticles for 12 h (Fig. 4A). Both cells were incubated for 24 h, it can be seen that the maturation rate of BMDCs in the mEHGZ-treated group is 33.3%, three times of that in the EPI-treated group (Fig. 4B), indicating that mEHGZ-treated 4T1 cells release a high level of tumor-related antigens and DAMPs to induce maturation of BMDCs.

3.6. In vivo immune activation

The released tumor-associated antigens and DAMPs after ICD of tumor cells promote DCs maturation and CTLs infiltration, activating the tumor immune microenvironment. Anti-PD-L1 antibody can bind to PD-1 expressed on T cells to mediate the “immune escape” [43], but its therapeutic effect is not very potent against tumor cells, especially those with an immunosuppressive microenvironment. It has been demonstrated that anti-PD-L1 antibody in combination with ICD can enhance its tumor-killing effect [44,45]. DCs present and process antigens to T cells to activate the innate and adaptive immune, and DCs maturation and cytokines secretion are two essential indicators for T cell activation and the cell-killing therapeutic effect. Mice were treated three times with EPI, EZ, GHZ, EHGZ, mEHGZ, anti-PD-L1 antibody, and mEHGZ + anti-PD-L1 antibody, they were sacrificed to analyze the immune-relevant cells three days after the last treatment.

The percentage of mature DCs, $CD11c^+CD80^+CD86^+$, is 36.1% after treatment with mEHGZ + anti-PD-L1 antibody, compared with 15.4% in the EPI-treated group, 17.1% in the EZ-treated group, 13.7% in the GHZ-treated group, 20.7% in the EHGZ-treated group, and 14.9% in the group treated with the antibody alone (Fig. 4C and Fig. S15), supporting that the treatment with mEHGZ and anti-PD-L1 antibody induces a significant level of DCs maturation in tumors. A similar result of promoting DCs maturation is found in lymph nodes after treatment with mEHGZ + anti-PD-L1 antibody (Fig. S16). These encouraging results can be ascribed to synergistic action of mEHGZ and the antibody. mEHGZ is able to induce ICD to evoke strong immune responses, and potent ICD is supported with a high level of CRT exposure on the cell membrane on the tumor slices of the treated mice (Fig. 4D). The anti-PD-L1 antibody is able to block the PD-L1 and PD-1 axis to enhance the chemotherapeutic effect. Cytokines play an essential role in eliciting immune responses [46]. For example, IFN-γ is a key mediator of Th1 cells [47], and TNF-α regulates the function of immune cells [48]. According to the ELISA assay results (Fig. 4E–G), the IFN-γ concentration is about 263.50 pg/mL in the mice group treated with mEHGZ, and it is 129.23 pg/mL in the EPI-treated group, while it increases to 380.44 pg/mL when the mice were synergistically treated with mEHGZ and the antibody, suggesting robust T cell-mediated immune responses are elicited. Meanwhile, TNF-α and IL-6 in the mEHGZ + anti-PD-L1 antibody treated group are upregulated and their concentrations are 2.5 and 6.4 folds of those in the EPI-treated group.

$CD8^+$ T cells are the main workforce in the immune system to battle with tumors, and the number of $CD8^+$ T cells is closely associated with the efficiency of inducing immune responses (Fig. 5A) [49]. The percentage of $CD8^+$ T cells in the tumor, lymph node, and spleen were analyzed, and the ratios in these tissues are presented in Fig. 5B–E (gating strategies are shown in Figs. S17 and S18). The $CD8^+$ T cell ratio increases from 1.83% in the EPI-treated group to 33.0% in the group treated with mEHGZ + anti-PD-L1 antibody, and this combinational treatment results in nearly 18-fold amplification of the number of $CD8^+$ T cells in the tumor (Fig. 5B and C). A similar increase in the percentage of $CD8^+$ T cells in the spleen and lymph nodes confirms the immune system is dynamically evoked (Figs. S19 and S20). The percentage of $CD8^+$ T cells in the spleen and lymph nodes is 10.5% and 16.5% in the mice treated with EPI, respectively, and it increases to 44.0% and 45.4% in the group treated with mEHGZ + anti-PD-L1 antibody (Fig. 5D and E). These results suggest that mEHGZ could induce ICD to release antigens, and these antigens are effectively engulfed by DCs and then presented to T cells to activate the immune system for enhancement in CTLs infiltration into the tumor. The immunofluorescence slices also support that the number of $CD8^+$ T cells infiltrated into the tumor is distinctively upregulated (Fig. 5F). After blocked $CD8^+$ T cell via intraperitoneal injection anti-CD8 antibody, the therapeutic effect of mEHGZ combination with anti-PD-L1 was weaker than in the immunocompetent mice (Fig. S21), showing $CD8^+$ T cells play important role in killing tumor cells. The treatment with mEHGZ+anti-PD-L1 antibody efficiently triggers the infiltration of IFN-γ^+ $CD8^+$ T cells into the tumor. 31.2% of IFN-γ^+ $CD8^+$ T cells is seen after the combinational treatment, which is 11.5 folds higher than that in the EPI-treated group (Fig. 5G and H). These results confirm that the synergistic treatment with mEHGZ and anti-PD-L1 antibody could induce vigorous *in vivo* adaptive immune responses.

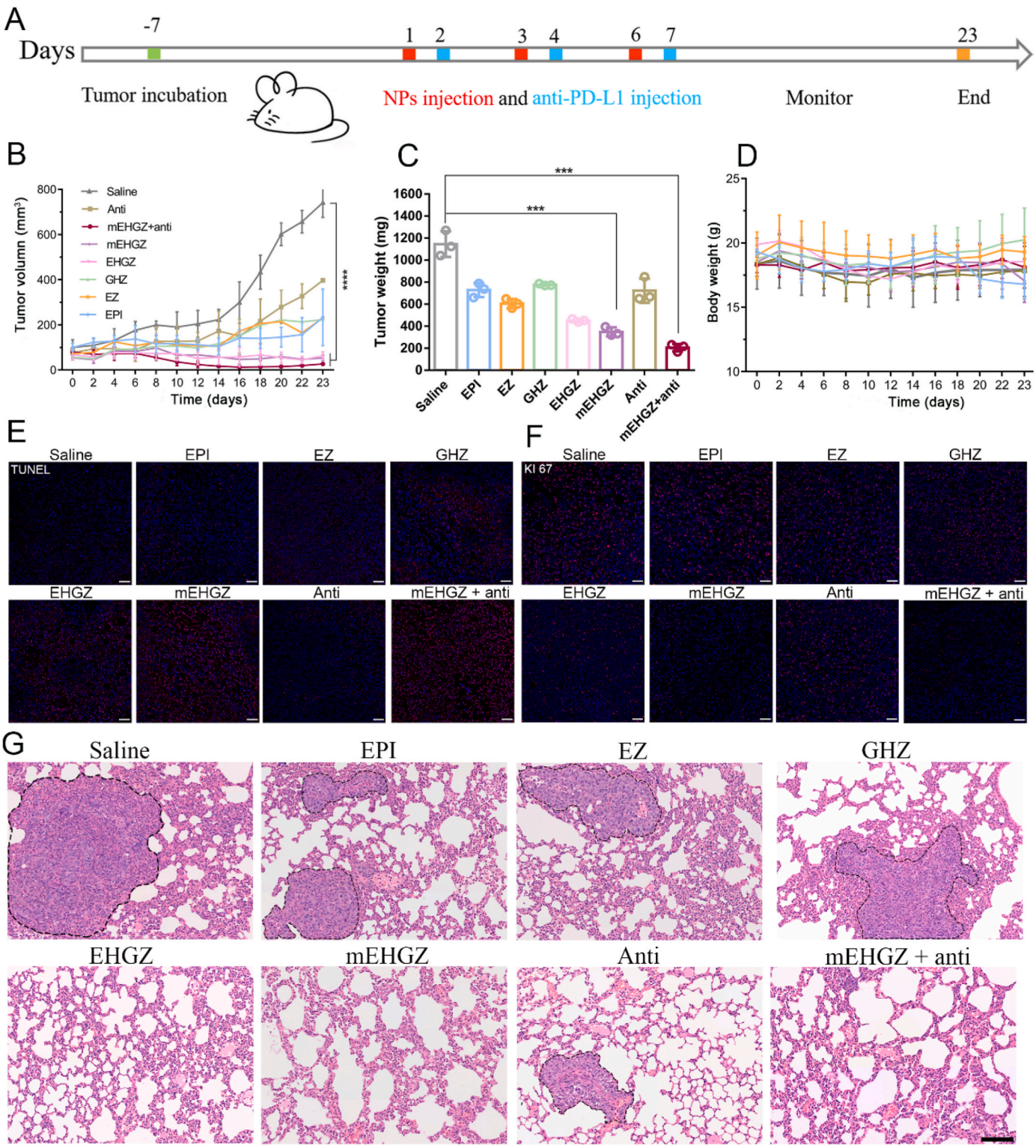

Fig. 6. *In vivo* anti-tumor effect in a 4T1-bearing mice model after treatment with mEHGZ combined with anti-PD-L1 antibody. A) Schematic diagram of the therapeutic schedule. The mice were intratumorally injected with EPI, EZ, GHZ, EHGZ, mEHGZ, anti-PD-L1 antibody, and mEHGZ + anti-PD-L1 antibody at an EPI dose of 3 mg/kg or intraperitoneal administrated with anti PD-L1 antibody of 100 μg, saline was uses as a blank control (n = 5). B) Tumor growth curves of mice after different treatments. C) Tumor weights after different treatments on day 24. D) Changes in the mice body weights in each experimental group. E-F) TUNEL and KI67 staining of the tumor tissue after different treatments (scale bar = 50 μm). G) H&E staining of lung tissues at the end of the anti-tumor experiment (scale bar = 100 μm). Data are represented as means ± SD. *$p < 0.05$, **$p < 0.01$, ***$p < 0.001$, ****$p < 0.0001$.

3.7. Anti-tumor therapeutic effect of mEHGZ nanoparticles

4T1-bearing mice were used to evaluate the *in vivo* anti-tumor effect of mEHGZ nanoparticles. EPI, EZ, GHZ, EHGZ, and saline were used as controls. After treatment of the mice three times every two days (Fig. 6A), EPI treatment barely suppresses tumor growth, while intervention with EHGZ and mEHGZ nanoparticles leads to pronounced delay in tumor growth, which may be ascribed to the elevated ER stress and the amplified ICD effect. Treatment with anti-PD-L1 antibody does not have an obvious effect on inhibition of tumor growth, while remarkable shrinkage of tumors is seen in mice after administration of anti-PD-L1 antibody combined with mEHGZ nanoparticles (Fig. 6B), which indicates that induced tumor cell death as well as an activated tumor immune microenvironment by mEHGZ nanoparticles could favorably potentiate the treatment effect of anti-PD-L1 antibody. Tumors were harvested and weighed at the end of the treatments. The tumor weights are consistent with the tumor volumes and the tumor in the group treated with mEHGZ + anti-PD-L1 antibody is the lightest, confirming this combinational treatment could effectively inhibit tumor cell proliferation (Fig. 6C). Treatment with mEHGZ and the anti-PD-L1 antibody displays the highest tumor growth inhibition rate of 82.02%, while 36.41% in the group after EPI treatment (Fig. S22). There was no significant body weight change during treatment with EHGZ or mEHGZ (Fig. 6D), indicating that negligible systemic toxicity of the constructed nanosystem. However, the EPI-treated mice lose their weights since day 16 due to the adverse effect induced by this therapeutic agent. There are no obvious pathologic changes in H&E staining slices of main organs, such as heart, liver, spleen and kidney, in mice treated with EHGZ, mEHGZ, mEHGZ + anti-PD-L1 antibody, suggesting that the self-amplified delivery system has excellent safety and biocompatibility (Fig. S23). Meanwhile, the remarkable treatment effect is also confirmed from the TUNEL and KI67 staining tumor sections (Fig. 6E and F). The tumor tissue in the group treated with mEHGZ + anti-PD-L1 antibody contains the highest ratio of dead cells and the KI67 signal is the weakest, suggesting significant apoptosis of tumor cells and severe damage of tumor cells proliferation. Impressively, metastatic nodules in the hematoxylin-eosin (H&E) staining lung sections are barely detectable in the groups treated with mEHGZ or mEHGZ + anti-PD-L1 antibody since induced potent immune responses prevent pulmonary metastasis, while lung metastasis are seen in these groups treated with EPI, EZ and GHZ, which are circled in Fig. 6G. Furthermore, mEHGZ displays a potent anti-tumor effect in the CT26-bearing mice (Fig. S24). The tumor growth weight is reduced from 3449.54 mg in the blank group to 1020.34 mg and 416.24 mg after treatment with EPI and mEHGZ, respectively. Therefore, mEHGZ could be a promising nanosystem for effectively inducing ICD to activate the tumor immune microenvironment and boost the therapeutic effect of anti-PD-L1 antibody.

4. Conclusion

In summary, we have successfully engineered a self-amplified biomimetic nanosystem, mEHGZ, in which EPI, Gox and hemin were loaded into ZIF-8 nanoparticles and the nanoparticles were coated with tumor cell membrane with over-expressed CRT. Homologous recognition of tumor cell membrane facilitates a high uptake efficiency of mEHGZ nanoparticles by 4T1 cells. CRT on the cell membrane of mEHGZ nanoparticles as an immune adjuvant promotes BMDCs and RAW 264.7 cells maturation. After endocytosis, the released EPI as an ICD inducer from mEHGZ in response to a low pH stimulates tumor cell death, releasing antigens and DAMPs to enhance the immunogenicity. Gox oxidizes glucose to reduce energy supply to tumor cells as well as produce H_2O_2 that reacts with co-released hemin to generate cytotoxic •OH and deplete intracellular GSH. The excess generated ROS exert a great level of stress to the ER and the ICD effect is significantly strengthened, which is supported with CRT exposure on the cell membrane, HMGB1 transfer to the cytoplasm and ATP release. This potent ICD induces DCs maturation and $CD8^+$ T cells infiltration to the tumor tissue for adaptive immune responses, which creates an immune-activated microenvironment. In this microenvironment, tumor cells become sensitive to the treatment with anti-PD-L1 antibody, and effective inhibition of tumor growth and restricted tumor lung metastasis are achieved in a 4T1 tumor-bearing mice model after treatment with an anti-PD-L1 antibody and mEHGZ. Thus, this nanosystem could be a promising nanoplatform to act as a nanovaccine to enhance the antigenicity and adjuvanticity and boost the treatment potency of anti-PD-L1 antibody for cancers including TNBC.

CRediT authorship contribution statement

Zhilin Li: Conceptualization, Methodology, Formal analysis, Investigation, Writing – original draft, Visualization. **Hao Cai:** Methodology, Formal analysis, Investigation, Funding acquisition. **Zhiqian Li:** Methodology, Investigation. **Long Ren:** Methodology, Formal analysis. **Xuelei Ma:** Supervision. **Hongyan Zhu:** Supervision, Project administration. **Qiyong Gong:** Supervision, Project administration. **Hu Zhang:** Writing – review & editing. **Zhongwei Gu:** Supervision, Project administration. **Kui Luo:** Supervision, Funding acquisition, Project administration, Resources, Writing – review & editing.

Declaration of competing interest

The authors declare that they have no known competing financial interests or personal relationships that could have appeared to influence the work reported in this paper.

Acknowledgements

This work was supported by National Natural Science Foundation of China (52073193, 51873120 and 81621003), and 1·3·5 Project for Disciplines of Excellence, West China Hospital, Sichuan University (ZYJC21013). Thanks to Sisi Wu, Hongying Chen, Zhiqian Li, Yu Ding, Xuemei Chen, Li Fu, Huaiqiang Sun, Shenglan You and Qing Yang (Research Core Facility, West China Hospital, Sichuan University) for their help in cell studies and histological studies. Thanks to Wentong Meng and Xue Li (Laboratory of Stem Cell Biology, West China Hospital, Sichuan University) for work in flow cytometer.

Appendix A. Supplementary data

Supplementary data to this article can be found online at https://doi.org/10.1016/j.bioactmat.2022.08.028.

References

[1] I. Mellman, G. Coukos, G. Dranoff, Cancer immunotherapy comes of age, Nature 480 (2011) 480–489.
[2] J. Nam, S. Son, K.S. Park, W. Zou, L.D. Shea, J.J. Moon, Cancer nanomedicine for combination cancer immunotherapy, Nat. Rev. Mater. 4 (2019) 398–414.
[3] S.L. Topalian, J.M. Taube, R.A. Anders, D.M. Pardoll, Mechanism-driven biomarkers to guide immune checkpoint blockade in cancer therapy, Nat. Rev. Cancer 16 (2016) 275–287.
[4] P. Sharma, S. Hu-Lieskovan, J.A. Wargo, A. Ribas, Primary, adaptive, and acquired resistance to cancer immunotherapy, Cell 168 (2017) 707–723.
[5] M.J. Smyth, S.F. Ngiow, A. Ribas, M.W. Teng, Combination cancer immunotherapies tailored to the tumour microenvironment, Nat. Rev. Clin. Oncol. 13 (2016) 143–158.
[6] Y. Li, X. Liu, X. Zhang, W. Pan, N. Li, B. Tang, Immunogenic cell death inducers for enhanced cancer immunotherapy, Chem. Commun. 57 (2021) 12087–12097.
[7] G. Kroemer, L. Galluzzi, O. Kepp, L. Zitvogel, Immunogenic cell death in cancer therapy, Annu. Rev. Immunol. 31 (2013) 51–72.
[8] J. Fucikova, O. Kepp, L. Kasikova, G. Petroni, T. Yamazaki, P. Liu, L. Zhao, R. Spisek, G. Kroemer, L. Galluzzi, Detection of immunogenic cell death and its relevance for cancer therapy, Cell Death Dis. 11 (2020) 1–13.
[9] A. Banstola, K. Poudel, J.O. Kim, J.H. Jeong, S. Yook, Recent progress in stimuli-responsive nanosystems for inducing immunogenic cell death, J. Control. Release 337 (2021) 505–520.

[10] G. Kroemer, C. Galassi, L. Zitvogel, L. Galluzzi, Immunogenic cell stress and death, Nat. Immunol. 23 (2022) 487–500.
[11] X. Duan, C. Chan, W. Han, N. Guo, R.R. Weichselbaum, W. Lin, Immunostimulatory nanomedicines synergize with checkpoint blockade immunotherapy to eradicate colorectal tumors, Nat. Commun. 10 (2019).
[12] Y. Chao, C. Liang, H. Tao, Y. Du, D. Wu, Z. Dong, Q. Jin, G. Chen, J. Xu, Z. Xiao, Q. Chen, C. Wang, J. Chen, Z. Liu, Localized cocktail chemoimmunotherapy after in situ gelation to trigger robust systemic antitumor immune responses, Sci. Adv. 6 (2020) eaaz4204.
[13] F. Zhou, B. Feng, H. Yu, D. Wang, T. Wang, Y. Ma, S. Wang, Y. Li, Tumor microenvironment-activatable prodrug vesicles for nanoenabled cancer chemoimmunotherapy combining immunogenic cell death induction and CD47 blockade, Adv. Mater. 31 (2019), 1805888.
[14] W. Yang, G. Zhu, S. Wang, G. Yu, Z. Yang, L. Lin, Z. Zhou, Y. Liu, Y. Dai, F. Zhang, In situ dendritic cell vaccine for effective cancer immunotherapy, ACS Nano 13 (2019) 3083–3094.
[15] F. Sun, Q. Zhu, T. Li, M. Saeed, Z. Xu, F. Zhong, R. Song, M. Huai, M. Zheng, C. Xie, L. Xu, H. Yu, Regulating glucose metabolism with prodrug nanoparticles for promoting photoimmunotherapy of pancreatic cancer, Adv. Sci. 8 (2021), 2002746.
[16] H. Deng, Z. Zhou, W. Yang, L.S. Lin, S. Wang, G. Niu, J. Song, X. Chen, Endoplasmic reticulum targeting to amplify immunogenic cell death for cancer immunotherapy, Nano Lett. 20 (2020) 1928–1933.
[17] D.V. Krysko, A.D. Garg, A. Kaczmarek, O. Krysko, P. Agostinis, P. Vandenabeele, Immunogenic cell death and DAMPs in cancer therapy, Nat. Rev. Cancer 12 (2012) 860–875.
[18] Z. Tang, Y. Liu, M. He, W. Bu, Chemodynamic therapy: tumour microenvironment-mediated Fenton and fenton-like reactions, Angew. Chem. Int. Edit. 58 (2019) 946–956.
[19] L.H. Fu, C. Qi, Y.R. Hu, J. Lin, P. Huang, Glucose oxidase-instructed multimodal synergistic cancer therapy, Adv. Mater. 31 (2019), 1808325.
[20] W. Sang, Z. Zhang, Y. Dai, X. Chen, Recent advances in nanomaterial-based synergistic combination cancer immunotherapy, Chem. Soc. Rev. 48 (2019) 3771–3810.
[21] H. Mei, S. Cai, D. Huang, H. Gao, J. Cao, B. He, Carrier-free nanodrugs with efficient drug delivery and release for cancer therapy: from intrinsic physicochemical properties to external modification, Bioact. Mater. 8 (2022) 220–240.
[22] F. Oroojalian, M. Beygi, B. Baradaran, A. Mokhtarzadeh, M.A. Shahbazi, Immune cell membrane-coated biomimetic nanoparticles for targeted cancer therapy, Small 17 (2021), e2006484.
[23] A.P. Johnson, C. Sabu, K.P. Nivitha, R. Sankar, V.K. Ameena Shirin, T.K. Henna, V. R. Raphey, H.V. Gangadharappa, S. Kotta, K. Pramod, Bioinspired and biomimetic micro- and nanostructures in biomedicine, J. Control. Release 343 (2022) 724–754.
[24] W. Zhang, M. Zhao, Y. Gao, X. Cheng, X. Liu, S. Tang, Y. Peng, N. Wang, D. Hu, H. Peng, Biomimetic erythrocytes engineered drug delivery for cancer therapy, Chem. Eng. J. 433 (2021), 133498.
[25] S.S. Kunde, S. Wairkar, Platelet membrane camouflaged nanoparticles: biomimetic architecture for targeted therapy, Int. J. Pharm. 598 (2021), 120395.
[26] G. Deng, Z. Sun, S. Li, X. Peng, W. Li, L. Zhou, Y. Ma, P. Gong, L. Cai, Cell-membrane immunotherapy based on natural killer cell membrane coated nanoparticles for the effective inhibition of primary and abscopal tumor growth, ACS Nano 12 (2018) 12096–12108.
[27] Z. Duan, Q. Luo, X. Dai, X. Li, L. Gu, H. Zhu, X. Tian, H. Zhang, Q. Gong, Z. Gu, Synergistic therapy of a naturally inspired glycopolymer-based biomimetic nanomedicine harnessing tumor genomic instability, Adv. Mater. 33 (2021), 2104594.
[28] Z. Zeng, K. Pu, Improving cancer immunotherapy by cell membrane-camouflaged nanoparticles, Adv. Funct. Mater. 30 (2020), 2004397.
[29] A.V. Kroll, R.H. Fang, Y. Jiang, J. Zhou, X. Wei, C.L. Yu, J. Gao, B.T. Luk, D. Dehaini, W. Gao, L. Zhang, Nanoparticulate delivery of cancer cell membrane elicits multiantigenic antitumor immunity, Adv. Mater. 29 (2017), 1703969.
[30] C. Xu, Y. Jiang, Y. Han, K. Pu, R. Zhang, A polymer multicellular nanoengager for synergistic NIR-II photothermal immunotherapy, Adv. Mater. 33 (2021), e2008061.
[31] Y. Pan, Y. Liu, G. Zeng, L. Zhao, Z. Lai, Rapid synthesis of zeolitic imidazolate framework-8 (ZIF-8) nanocrystals in an aqueous system, Chem. Commun. 47 (2011) 2071–2073.
[32] B. Bahmani, H. Gong, B.T. Luk, K.J. Haushalter, E. DeTeresa, M. Previti, J. Zhou, W. Gao, J.D. Bui, L. Zhang, Intratumoral immunotherapy using platelet-cloaked nanoparticles enhances antitumor immunity in solid tumors, Nat. Commun. 12 (2021) 1–12.
[33] H. Zheng, Y. Zhang, L. Liu, W. Wan, P. Guo, A.M. Nyström, X. Zou, One-pot synthesis of metal-organic frameworks with encapsulated target molecules and their applications for controlled drug delivery, J. Am. Chem. Soc. 138 (2016) 962–968.
[34] M. Obeid, A. Tesniere, F. Ghiringhelli, G.M. Fimia, L. Apetoh, J.-L. Perfettini, M. Castedo, G. Mignot, T. Panaretakis, N. Casares, Calreticulin exposure dictates the immunogenicity of cancer cell death, Nat. Med. 13 (2007) 54–61.
[35] L. Liu, X. Bai, M.V. Martikainen, A. Kårlund, M. Roponen, W. Xu, G. Hu, E. Tasciotti, V.P. Lehto, Cell membrane coating integrity affects the internalization mechanism of biomimetic nanoparticles, Nat. Commun. 12 (2021) 5726.
[36] Z. Chen, P. Zhao, Z. Luo, M. Zheng, H. Tian, P. Gong, G. Gao, H. Pan, L. Liu, A. Ma, H. Cui, Y. Ma, L. Cai, Cancer cell membrane-biomimetic nanoparticles for homologous-targeting dual-modal imaging and photothermal therapy, ACS Nano 10 (2016) 10049–10057.
[37] H. Sun, J. Su, Q. Meng, Q. Yin, L. Chen, W. Gu, P. Zhang, Z. Zhang, H. Yu, S. Wang, Y. Li, Cancer-cell-biomimetic nanoparticles for targeted therapy of homotypic tumors, Adv. Mater. 28 (2016) 9581–9588.
[38] G.S. Hotamisligil, Endoplasmic reticulum stress and the inflammatory basis of metabolic disease, Cell 140 (2010) 900–917.
[39] F. Weinberg, N. Ramnath, D. Nagrath, Reactive oxygen species in the tumor microenvironment: an overview, Cancers 11 (2019) 1191.
[40] A. Bansal, M.C. Simon, Glutathione metabolism in cancer progression and treatment resistance, J. Cell Biol. 217 (2018) 2291–2298.
[41] T. Panaretakis, O. Kepp, U. Brockmeier, A. Tesniere, A.C. Bjorklund, D. C. Chapman, M. Durchschlag, N. Joza, G. Pierron, P. Van Endert, Mechanisms of pre-apoptotic calreticulin exposure in immunogenic cell death, EMBO J. 28 (2009) 578–590.
[42] X. Xiong, J. Zhao, J. Pan, C. Liu, X. Guo, S. Zhou, Personalized nanovaccine coated with calcinetin-expressed cancer cell membrane antigen for cancer immunotherapy, Nano Lett. 21 (2021) 8418–8425.
[43] J.X. Yu, J.P. Hodge, C. Oliva, S.T. Neftelinov, V.M. Hubbard-Lucey, J. Tang, Trends in clinical development for PD-1/PD-L1 inhibitors, Nat. Rev. Drug Discov. 19 (2020) 163–164.
[44] R. Alzeibak, T.A. Mishchenko, N.Y. Shilyagina, I.V. Balalaeva, M.V. Vedunova, D. V. Krysko, Targeting immunogenic cancer cell death by photodynamic therapy: past, present and future, J. Immunother. Cancer 9 (2021), e001926.
[45] C. Xu, Y. Jiang, Y. Han, K. Pu, R. Zhang, A polymer multicellular nanoengager for synergistic NIR-II photothermal immunotherapy, Adv. Mater. 33 (2021), 2008061.
[46] S. Lee, K. Margolin, Cytokines in cancer immunotherapy, Cancers 3 (2011) 3856–3893.
[47] M.B. Fuertes, A.K. Kacha, J. Kline, S.R. Woo, D.M. Kranz, K.M. Murphy, T. F. Gajewski, Host type I IFN signals are required for antitumor $CD8^+$ T cell responses through CD8 α^+ dendritic cells, J. Exp. Med. 208 (2011) 2005–2016.
[48] Q. Luo, L. Zhang, C. Luo, M.J.C.L. Jiang, Emerging strategies in cancer therapy combining chemotherapy with immunotherapy, Cancer Lett. 454 (2019) 191–203.
[49] Q. Luo, Z. Duan, X. Li, L. Gu, L. Ren, H. Zhu, X. Tian, R. Chen, H. Zhang, Q. Gong, Branched polymer-based redox/enzyme-activatable photodynamic nanoagent to trigger STING-dependent immune responses for enhanced therapeutic effect, Adv. Funct. Mater. 32 (2022), 2110408.